

Article

Characteristics of AISI 420 Stainless Steel Modified by Low-Temperature Plasma Carburizing with Gaseous Acetone

Ruiliang Liu ^{1,*}  and Mufu Yan ²

¹ Key Laboratory of Superlight Material and Surface Technology of Ministry of Education, College of Material Science and Chemical Engineering, Harbin Engineering University, Harbin 150001, China

² National Key Laboratory for Precision Hot Processing of Metals, School of Materials Science and Engineering, Harbin Institute of Technology, Harbin 150001, China; yanmufu@hit.edu.cn

* Correspondence: liuruiliang@hrbeu.edu.cn; Tel.: +86-451-8251-8731

Received: 27 December 2018; Accepted: 23 January 2019; Published: 26 January 2019



Abstract: In this research work, low-temperature carburizing of AISI 420 martensitic stainless steel was conducted at 460 °C for different amounts of time using an acetone source. The microstructure and phase structure of the carburized layers were characterized by optical microscope and X-ray diffraction. The properties of the carburized layers were tested with a microhardness tester and an electrochemical workstation. The results indicate uniform layers are formed on martensitic stainless steel surfaces, and the carburized layers are mainly composed of carbon “expanded” α (α_C) and Fe_3C phases. The property tests indicated that after plasma-carburizing, the hardness of the stainless steel surface can reach up to 850 HV_{0.1}. However, the corrosion resistance of stainless steel decreased slightly, and the corrosion characteristic of stainless steel was altered from pitting to general corrosion. The semiconductor characteristic of the passivation film on stainless steel was transformed from the *p*-type for untreated specimens to the *n*-type for carburized specimens.

Keywords: martensitic stainless steel; low temperature plasma carburizing; carbon source; microstructure; corrosion behavior

1. Introduction

Stainless steel is widely used for its inherent corrosion resistance. However, unmodified stainless steel can be problematic when it is used in moving parts in some harsh environments, such as aerospace, electric power stations, ships, and ocean engineering [1]. At present, surface modification has become an important solution to improve surface properties of stainless steel to meet demands in the harsh environments mentioned above [2–4]. There are various surface modification methods that have been utilized to improve the properties of stainless steel, of which thermo-chemical diffusion treatment strategies have drawn significant consideration for their simple process, low cost, and other advantages [5]. Among these, low-temperature nitriding, carburizing, and nitrocarburizing treatments are the commonly used processes that can improve the hardness and wear-resistance of stainless steels without reducing their corrosion resistance [6,7]. Thus, these treatments have received extensive research attention [7–9].

Regarding the low-temperature carburization of stainless steel, most research is focused on studying the microstructure and mechanical properties of the modified layers [10–14]. A literature survey indicated that the corrosion property studies of the carburized layers were mainly conducted on austenitic stainless steels [15–17], and only a few were related to the carburized layers on martensitic stainless steels [18,19]. Notably, most low-temperature carburization of stainless steel was conducted using CH₄ or CO gas carbon sources [10–14,20].

Interestingly, when bearing steel (M50NiL) was plasma-carburized with an acetone source, diamond-like carbon/Fe₃C-containing carburized layers were formed, and the layers possessed self-lubricating and anti-corrosion properties [21–23]. Recently, authors have also proved that the low-temperature carburization of AISI 431 stainless steel could be successfully conducted with gaseous acetone. The carburized layer thickness could reach up to 45 μm with a hardness higher than 1051 HV_{0.1}, while corrosion resistance decreased only slightly [24]. Since the alloying elements in stainless steel have an important influence on the microstructure and properties of the low-temperature plasma surface alloyed layer [25], there is great need to study the plasma carburization of other kinds of stainless steels with an acetone source.

Therefore, based on previous research [15–20], AISI 420 martensitic stainless steel was plasma-carburized at 460 °C for 4–12 h using an acetone source. Then, a preliminary study of the microstructure and properties of the carburized layer was conducted, and the effects of the alloy elements were especially considered. Since the corrosion resistance of the carburized layer is one of the important concerns for stainless steel, the present investigation primarily focused on the corrosion behaviors of the carburized layer.

2. Materials and Experimental Methods

Commercially available AISI 420 martensitic stainless steel with the chemical composition (wt %) of 0.16%–0.25% C, ≤0.60% Si, ≤0.80% Mn, ≤0.035% P, ≤0.030% S, ≤0.75% Ni, 12.0%–14.0% Cr, and Fe in balance was used in the present investigation. The as-received AISI 420 stainless steel rod was first machined to the size of Φ 25 mm × 5 mm, and then the steel was austenitized at 1050 °C for 1 h and oil-cooled.

Plasma-carburizing treatments were conducted in a 30 kW home-made pulse plasma multi-diffusing unit [9]. The process parameters were: temperature, 460 °C; time, 4–12 h; pressure, 200–300 Pa; voltage, 650 V; and carburizing atmosphere, H₂:CH₃COCH₃ = 4:1. Acetone (CH₃COCH₃) was heated into vapor and then inputted into the furnace along with hydrogen (H₂). The ageing treatment of stainless steel could be conducted simultaneously during plasma carburization.

The carburized specimens were cross-sectioned and set in bakelite, and then the cross section was grinded with 240–2000# sandpapers and polished with Al₂O₃ polishing powder. After that, the specimens were light-etched using Marble's reagent [9], and then were observed by a metallographic microscope (OM, CMM-33E, Shanghai Changfang Optical Instrument CO., LTD., Shanghai, China). The thicknesses of the carburized layers were roughly estimated based on OM observations because of an obvious boundary between layer and matrix, and then were proved by hardness profiles on the cross sections.

The identification of the phases present in the carburized layers was carried out by X'Pert Pro X-ray diffraction (PANalytical, Almelo, The Netherlands). Test conditions were: Cu Kα radiation (λ = 1.5406 nm); voltage, 40 kV; current, 40 mA; speed, 0.7°/s; and scanning range, 20–100°.

Surface hardness and cross-sectional hardness profile of the carburized specimens were obtained using a microhardness tester (HV-1000, Fangyuan Instrument CO., LTD., Jinan, China). The applied load was 100 gf, and the hold time was 15 s.

The corrosion behaviors of the carburizing layers were studied by the potentiodynamic polarization curves and electrochemical impedance spectroscopy (EIS) using electrochemical testing equipment (Chi660e, Shanghai Chenhua Instruments Co., Ltd., Shanghai, China) in 3.5 wt % NaCl solution. Based on the standard of GB/T 24196-2009 [26], the potentiodynamic polarization curves of the specimens were tested. A three-electrode system was also used in the present investigation, including the working electrode (W) of specimen, the auxiliary electrode (C) of a platinum wire, and the reference electrode (R) of a saturated calomel electrode (SCE). The size of the test surface was about 1 cm² in area. For polarization curve tests, scanning started from the open circuit potential of –300 mV with a scanning speed of 5 mV/s. Scanning stopped when the current density reached 10 mA/cm². In the EIS tests, the specimens were submerged in solution for 120 s under a voltage

of 250 mV to gain a stable passivation membrane. The excitation signal had a sine wave with an amplitude of 5 mV, and the test frequency was 10^{-2} – 10^5 Hz. Mott–Schottky (M – S) curve tests were used to characterize the semiconductor characteristics of the film formed on the carburized layer, where the test potential range was 1000–600 mV, and test speed was 50 mV/step.

3. Results and Discussion

3.1. Phase Structure of the Carburized Layer

The phase compositions of the carburized layers on AISI 420 stainless steel are shown in Figure 1. It is well-known that the only phase on an untreated steel surface is the α' -Fe phase. After plasma carburization, carbon “expanded” α' -Fe (α_C) phases and Fe_3C phases formed on the stainless steel surface. The α_C phase formation was evidenced by the broadening of the original martensite peaks and their displacement to lower angles [12,13,18]. Moreover, with the increase of carburizing time, the peak intensities of α_C phases showed almost no change. The phase composition in the carburized layer played an important role in the properties of the carburized layer, as shown in the following parts.

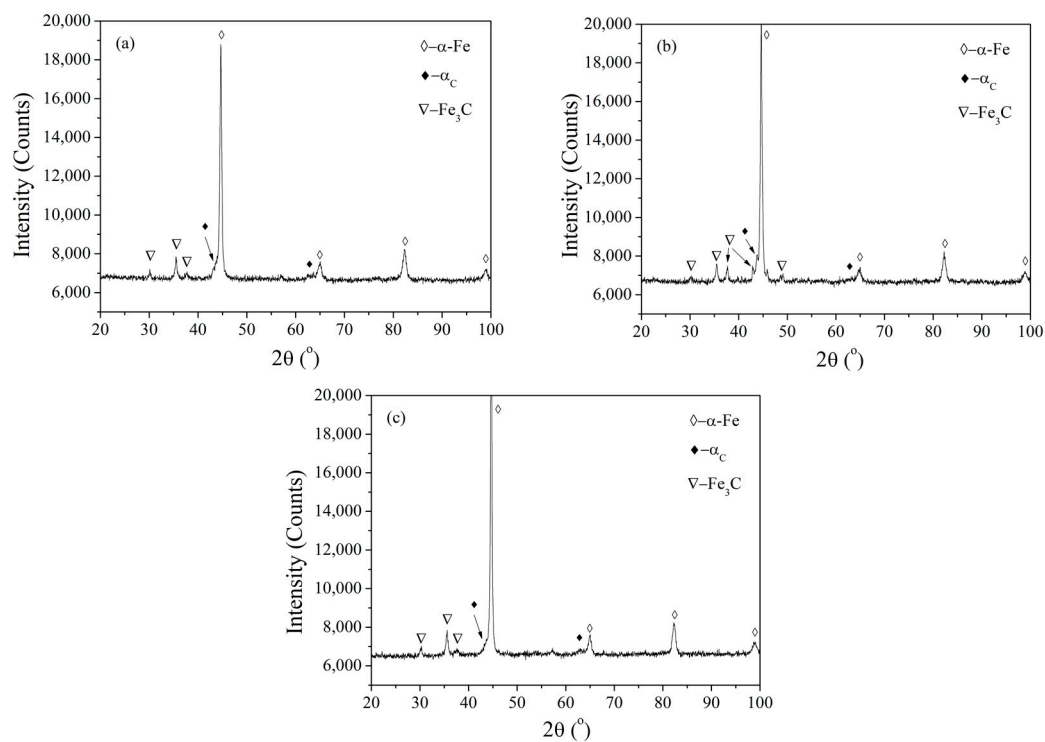


Figure 1. XRD patterns of AISI 420 stainless steel plasma carburized at 460 °C: (a) 4 h; (b) 8 h; and (c) 12 h.

3.2. Microstructure and Hardness Profile of the Carburized Layer

The cross-sectional optical micrographs and microhardness profiles of low-temperature-carburized layers on AISI 420 stainless steels are presented in Figure 2. One can see in Figure 2a–c that prominent plasma-carburized layers were formed on the stainless steel surfaces after light erosion, and the layer thickness increased with time. Based on the OM observation, the carburized layer thicknesses were determined to be about 26, 42, and 62 μ m for the specimens plasma-carburized at 460 °C for 4, 8, and 12 h, respectively. The layer thicknesses obtained on AISI 420 stainless steel were higher than those on AISI 431 stainless steel in the same plasma-carburizing condition [24]. The present investigation also proved that the alloying elements had obvious effects on the microstructures of the carburized layers, as shown in [25]. Moreover, the etchant (Marble’s reagent) did not attack the carburized layers, which is commonly an empirical indication of an improvement in corrosion resistance in the etching medium. However, when the carburizing time increased up to 12 h (Figure 2c), the microstructure

showed a porous state with some black spots, which can be caused by the precipitation and grain growth of the carbides [18,24].

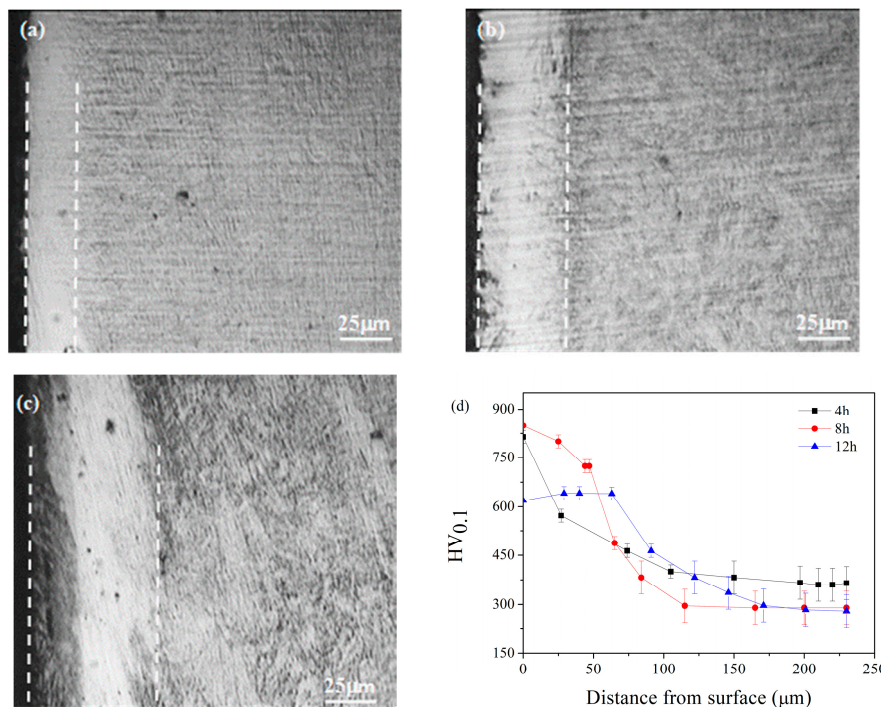


Figure 2. (a–c) Cross section microstructures. (d) Microhardness profiles of AISI 420 stainless steel plasma carburized at 460 °C for 4, 8, and 12 h.

As shown in References [21–23], a diamond-like carbon/Fe₃C-containing carburized layer could be formed on M50NiL steel after plasma-carburizing with acetone. The fine microstructure characterization of the carburized layer on AISI 420 stainless steel will be characterized in the near future.

In addition, it can be seen from Figure 2d that the surface hardness of stainless steel was improved after plasma carburizing. The surface hardnesses of the untreated, 4, 8, and 12 h treated specimens were about 300, 810, 850, and 620 HV_{0.1}, respectively. That is, the surface hardness of the stainless steel was improved up to 2.8 times more than that of the untreated steel, which should be attributed to the higher lattice distortion strengthening in “expanded” α'-Fe lattices [11] and high hardness of the Fe₃C phase. Moreover, the surface hardness increased first and then decreased with duration. The reasons for this could be mainly due to the grain growth of carbides and microstructure deterioration for the 12 h carburized layer, as shown in Figure 2c.

It can also be seen that the bulk hardnesses changed with time, which is almost in agreement with the ageing effect observed for each treatment temperature [9,12]. Thus, the ageing of the martensitic stainless steel can be conducted simultaneously with the plasma carburization treatment. Compared with the surface hardnesses of the carburized layers obtained on AISI 431 stainless steel under the same carburization conditions, the hardnesses did not show much variation between 4 and 12 h carburized layers, but the highest hardness decreased from 1050 to 850 HV_{0.1} [24]. Moreover, compared with AISI 420 stainless steel plasma carburized at 450 °C with a CH₄ source, the carburized layer thicknesses and hardnesses were almost the same and showed the same variation trends with the present investigation [12,13].

3.3. Corrosion Behavior of the Carburized Layer

Figure 3 shows the typical polarization curves of stainless steel carburized at 460 °C for 4–12 h, and the corresponding corrosion parameters are given in Table 1. It can be seen from Table 1 that for the untreated specimen and the specimens carburized for 4, 8, and 12 h, the corresponding corrosion potentials (E_{corr}) were -0.38 V (SCE), -0.56 V (SCE), -0.56 V (SCE), and -0.58 V (SCE), and the corrosion current densities were 3.19×10^{-6} A/cm², 2.54×10^{-5} A/cm², 1.99×10^{-5} A/cm², and 2.99×10^{-5} A/cm², respectively. Moreover, there was no obvious pitting phenomenon (i.e., no evident passivation region) for the carburized specimens. The corrosion resistance of the martensitic stainless steel was slightly worse than that of the untreated one, and the specimen carburized for 8 h had the better corrosion resistance at the present test condition, which is consistent with plasma carburization of AISI 431 stainless steel [24]. However, this disagrees with the corrosion test results obtained from low-temperature carburization of AISI 316 austenitic stainless steel [15,16]. The main reasons could be the multi-phase microstructure characteristics shown in XRD results, because the microstructure had a significant influence on the corrosion behavior of the steel [6,18]. In fact, some other researchers also found this kind of corrosion phenomenon in the low-temperature ion nitriding of martensitic stainless steel—for example, Corengia et al. [19] found that ion nitriding at 673–773 K (400–500 °C) reduced the corrosion resistance of AISI 410 martensitic stainless steel.

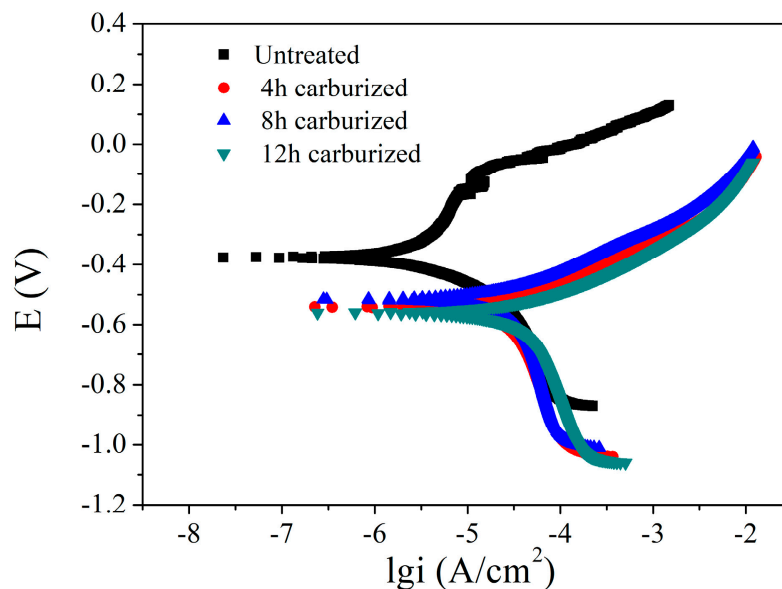


Figure 3. Polarization curves of AISI 420 stainless steel plasma carburized at 460 °C for 4–12 h.

Table 1. Parameters obtained from polarization curves of AISI 420 stainless steel plasma carburized at 460 °C for 4–12 h.

Specimen	E_{corr} (V)	I_{corr} (A/cm ²)
Untreated	-0.38	3.19×10^{-6}
4 h	-0.56	2.54×10^{-5}
8 h	-0.56	1.99×10^{-5}
12 h	-0.58	2.99×10^{-5}

To further study the stabilities of the passive films formed during corrosion of the carburized layer, EIS measurements were carried out. Figure 4 depicts the Nyquist and Bode curves of the untreated specimen and specimens plasma-carburized at 460 °C for 4–12 h. Electrical equivalent circuits were obtained based on ZView software (Version 3.0a), and the values of each part could be directly measured. The corresponding data are shown in Table 2. In the table, CPE is an abbreviation for constant phase angle element [27], the impedance value of which is the function of angle frequency (ω), and its amplitude angle is independent of frequency. There are two parameters: CPE-T and CPE-P. CPE-T is called double-layer capacitance, CPE-P is a dispersion index and is normally used to characterize dispersion effects. The simulation results of the percentage errors were within 5%, that is, the data-fitting results were good and the chosen model could be used to characterize the specimens' corrosion equivalent circuit. It can be seen from the figure that the impedance spectra were all a single capacitive arc with only one time constant. The bigger the capacitance arc radius, the higher the stability of the film [14]. The biggest capacitance arc radius, from the specimen carburized for 8 h, indicated that the passive film that formed on this specimen possessed the highest stability in a corrosive environment. These results are consistent with the plasma carburization of AISI 431 stainless steel [24].

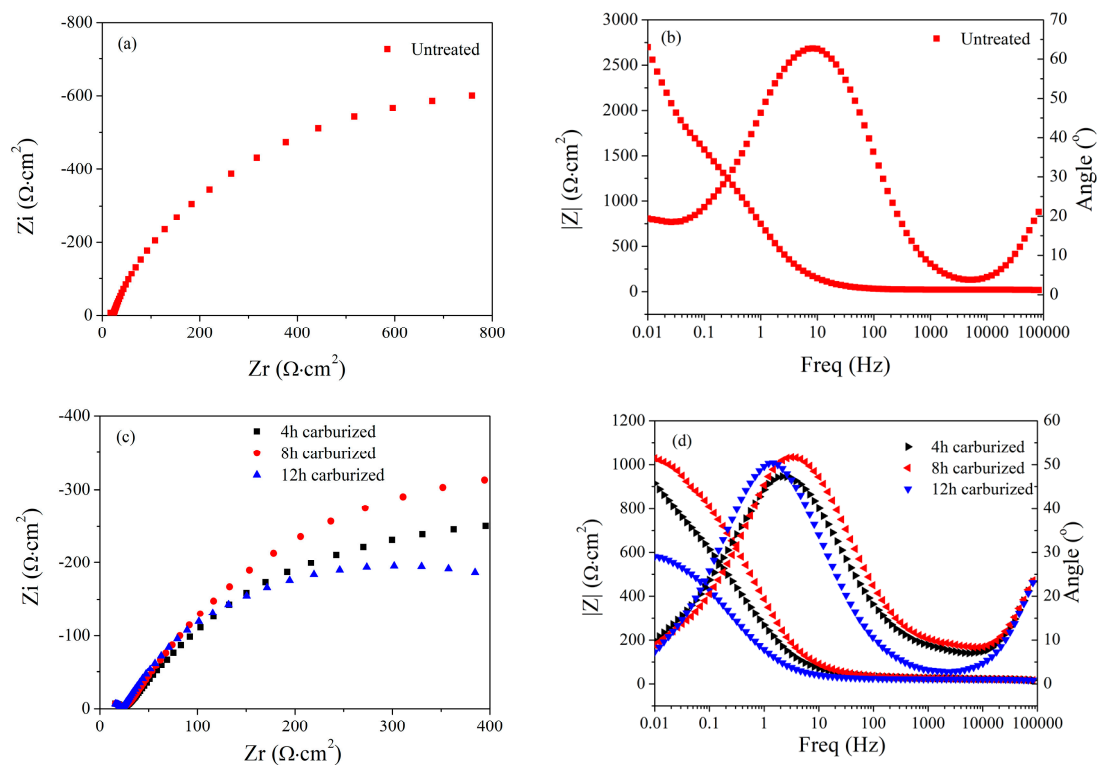


Figure 4. Nyquist and Bode plots of AISI 420 stainless steel. (a,b) Untreated specimen, (c,d) Carburized specimens.

Table 2. Fitting parameter values for the untreated and the carburized AISI 420 stainless steel. CPE-P: dispersion index; CPE-T: double-layer capacitance.

Specimen	R_s (Ω)		CPE-T (F)		CPE-P (F)		R_p (Ω)	
	Value	Error%	Value	Error%	Value	Error%	Value	Error%
Untreated	21.95	0.19	0.00023	0.5	0.84	0.13	1506	0.93
4 h	21.21	0.66	0.0015	1.38	0.62	0.59	1227	4.5
8 h	22.66	0.45	0.00078	0.99	0.68	0.35	1006	1.89
12 h	23.01	0.52	0.0016	1.24	0.72	0.52	786.5	3.41

In addition, it can be seen in Table 2 that for the untreated specimen, the membrane resistance (R_p) and the capacitance (CPE-T) were 1506 Ω and 0.00023 F. For the specimens plasma-carburized for 4, 8, and 12 h, the membrane resistances (R_p) were 1227, 1006, and 786.5 Ω , while the capacitances were 0.0015, 0.00078, and 0.0016 F, respectively. The larger the value of R_p , the smaller the corrosion rate of the film. All the above values indicated that, after plasma carburization at 460 °C, the stabilities of passive films formed on the specimens were all lower than those of untreated specimen, and decreased slightly with time. The passive film was the least stable for the stainless steel carburized for 12 h, which was likely due to the microstructure deterioration as shown before.

Finally, it should be pointed out that the corrosion resistance of the carburized layer showed a slight decrease under the present investigation condition. As such, optimization of the process parameters will be important work in the next steps, even though some reports also found that the low-temperature treatments were not necessary to keep or improve the corrosion resistance of stainless steels [19]. Considering that plasma processing parameters have an important influence on the microstructure of the carburized layers, deeper experiments are being conducted aiming to evaluate the effects of the temperature and acetone gas content to obtain better corrosion resistance.

Based on the Mott–Schottky (M–S) theory, it is well-known that the space charge layer capacitance (C) of the passivation film is a function of the electrode potential [15,16]. For an n-type semiconductor, the value of C can be represented by Equation (1):

$$\frac{1}{C^2} = \frac{2}{\epsilon\epsilon_0qN_d} \left(E - E_{fb} - \frac{kT}{q} \right) \quad (1)$$

For the *p*-type semiconductor, the value of C can be represented by Equation (2):

$$\frac{1}{C^2} = \frac{-2}{\epsilon\epsilon_0qN_a} \left(E - E_{fb} - \frac{kT}{q} \right) \quad (2)$$

where N_d is the carrier charge concentration of the donor and N_a is the carrier charge concentration of the acceptor.

According to the slope of the linear part in the M–S curve, the electronic structure type of the passive film can be determined. When the value is positive, it possesses the n-type semiconductor characteristic, otherwise, it possesses the *p*-type semiconductor characteristic [15,16]. The charge concentration of donor or acceptor in the surface space is directly proportional to the reciprocal of the slope of the M–S curve, and can be estimated by Equation (3):

$$N_d(N_a) = \frac{2}{e\epsilon\epsilon_0S} \quad (3)$$

Figure 5 plots the M–S curves of the untreated specimen and specimens plasma-carburized at 460 °C for 4–12 h. For the untreated specimen, the slope of the linear part (0.15–0.50 V) in the curve was negative, the film formed on the untreated specimen possessed the *p*-type semiconductor property, and the donor charge concentration was calculated to be about $2.59 \times 10^{22} \text{ cm}^{-3}$. On the other hand, for the specimens after plasma carburization at 460 °C, the slope of the linear parts (0.15–0.50 V) in the curves were all positive, which all corresponded to n-type semiconductor properties [24], and the donor charge concentrations for specimens carburized for 4, 8, and 12 h were calculated to be about 3.02×10^{21} , 2.56×10^{21} , and $6.66 \times 10^{21} \text{ cm}^{-3}$, respectively.

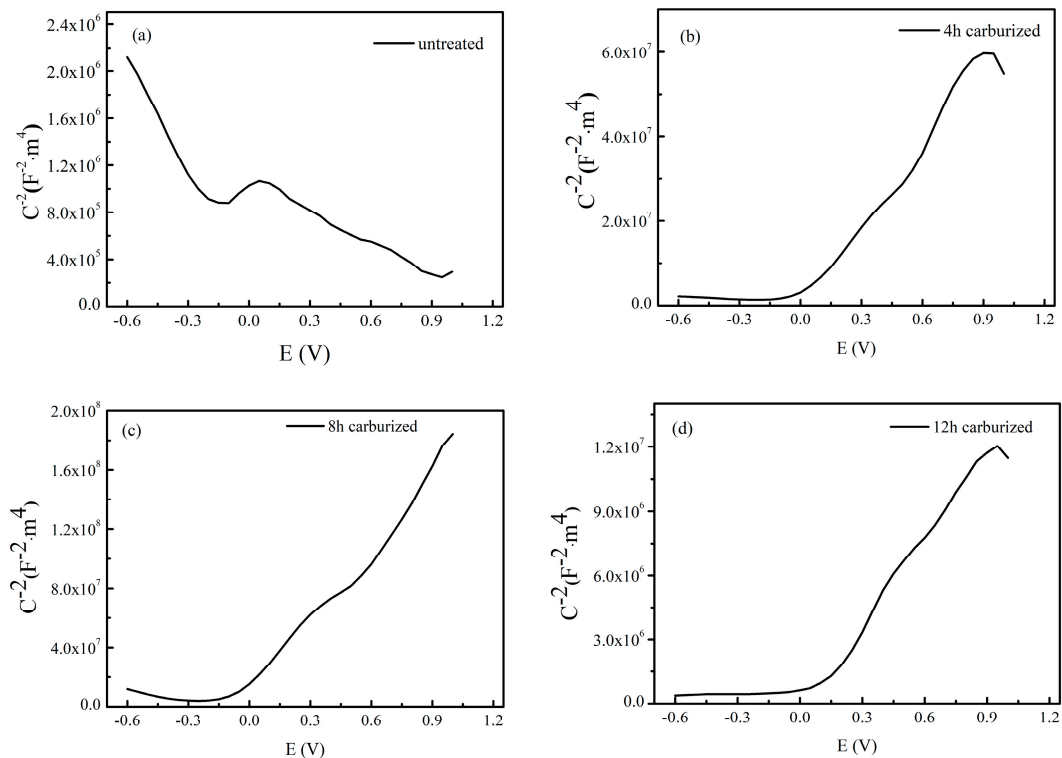


Figure 5. Mott–Schottky (M–S) plots of the untreated and the carburized AISI 420 stainless steel: (a) untreated; (b) 4 h carburized; (c) 8 h carburized; (d) 12 h carburized.

4. Conclusions

- After plasma carburization at 460 °C with gaseous acetone, uniform layers were formed on the AISI 420 martensitic stainless steel surface, and the carburized layer was mainly composed of carbon “expanded” α (α_c) and some Fe_3C phases.
- The hardness of the carburized layer on stainless steel could be improved up to 850 $\text{HV}_{0.1}$, which was about 2.8 times higher than that of the untreated one.
- The corrosion resistance of stainless steel after plasma carburization showed a slight decrease under the present test conditions, and the corrosion characteristic of the stainless steel was altered from pitting to general corrosion. The semiconductor characteristic of the passivation film on stainless steel was transformed from the p -type for the untreated specimen to the n -type for carburized specimens.

Author Contributions: Conceptualization, R.L.; Methodology, R.L.; Investigation, R.L.; Resource, R.L.; Data Curation, R.L. and M.F.; Writing-Original Draft Preparation, R.L. and M.F.; Writing and Editing, R.L. and M.F.; Supervision, R.L. and M.F.; Project Administration, R.L.; Funding Acquisition, R.L.

Funding: This research was funded by the National Natural Science Foundation of China (Nos. 51401062, 51871071).

Acknowledgments: The authors would like to thank A. Xu for his experimental assistance.

Conflicts of Interest: The authors declare no conflict of interest.

References

1. Bahrami, A.; Mousavi Anijdan, S.H.; Taheri, P.; Yazdan Mehr, M. Failure of AISI 304H stainless steel elbows in a heat exchanger. *Eng. Fail. Anal.* **2018**, *90*, 397–403. [[CrossRef](#)]
2. Sun, J.; Yao, Q. Fabrication of microalloy nitrided layer on low carbon steel by nitriding combined with surface nano-alloying pretreatment. *Coatings* **2016**, *6*, 63. [[CrossRef](#)]

3. Yamaguchi, T.; Hagino, H. Formation of a titanium-carbide-dispersed hard coating on austenitic stainless steel by laser alloying with a light-transmitting resin. *Vacuum* **2018**, *155*, 23–28. [[CrossRef](#)]
4. Adachi, S.; Ueda, N. Wear and corrosion properties of cold-sprayed AISI 316L coatings treated by combined plasma carburizing and nitriding at low temperature. *Coatings* **2018**, *8*, 456. [[CrossRef](#)]
5. Nikolov, K.; Bunk, K.; Jung, A.; Kaestner, P.; Bräuer, G.; Klages, C.-P. High-efficient surface modification of thin austenitic stainless steel sheets applying short-time plasma nitriding by means of strip hollow cathode method for plasma thermochemical treatment. *Vacuum* **2014**, *110*, 106–113. [[CrossRef](#)]
6. Li, Y.; He, Y.; Xiu, J.; Wang, W.; Zhu, Y.; Hu, B. Wear and corrosion properties of AISI 420 martensitic stainless steel treated by active screen plasma nitriding. *Surf. Coat. Technol.* **2017**, *329*, 184–192. [[CrossRef](#)]
7. Alphonsa, J.; Raja, V.S.; Mukherjee, S. Development of highly hard and corrosion resistant A286 stainless steel through plasma nitrocarburizing process. *Surf. Coat. Technol.* **2015**, *280*, 268–276. [[CrossRef](#)]
8. Kim, S.K.; Yoo, J.S.; Priest, J.M.; Fewell, M.P. Characteristics of martensitic stainless steel nitrided in a low-pressure RF plasma. *Surf. Coat. Technol.* **2003**, *163*, 380–385. [[CrossRef](#)]
9. Liu, R.; Qiao, Y.; Yan, M.; Fu, Y. Layer growth kinetics and wear resistance of martensitic precipitation hardening stainless steel plasma nitrocarburized at 460 °C with rare earth addition. *Met. Mater. Int.* **2013**, *19*, 1151–1157. [[CrossRef](#)]
10. Ernst, F.; Cao, Y.; Michal, G.M.; Heuer, A.H. Carbide precipitation in austenitic stainless steel carburized at low temperature. *Acta Mater.* **2007**, *55*, 1895–1906. [[CrossRef](#)]
11. Hummelshøj, T.S.; Christiansen, T.L.; Somers, M.A.J. Lattice expansion of carbon-stabilized expanded austenite. *Scripta Materialia* **2010**, *63*, 761–763. [[CrossRef](#)]
12. Scheuer, C.J.; Cardoso, R.P.; Zanetti, F.I.; Amaral, T.; Brunatto, S.F. Low-temperature plasma carburizing of AISI 420 martensitic stainless steel: Influence of gas mixture and gas flow rate. *Surf. Coat. Technol.* **2012**, *206*, 5085–5090. [[CrossRef](#)]
13. Scheuer, C.J.; Cardoso, R.P.; Mafra, M.; Brunatto, S.F. AISI 420 martensitic stainless steel low-temperature plasma assisted carburizing kinetics. *Surf. Coat. Technol.* **2013**, *214*, 30–37. [[CrossRef](#)]
14. Rovani, A.C.; Breganon, R.; De Souza, G.S.; Brunatto, S.F.; Pintaúde, G. Scratch resistance of low-temperature plasma nitrided and carburized martensitic stainless steel. *Wear* **2017**, *376–377*, 70–76. [[CrossRef](#)]
15. Sun, Y. Corrosion behaviour of low temperature plasma carburised 316L stainless steel in chloride containing solutions. *Corros. Sci.* **2010**, *52*, 2661–2670. [[CrossRef](#)]
16. Sun, Y. Depth-profiling electrochemical measurements of low temperature plasma carburised 316L stainless steel in 1 M H₂SO₄ solution. *Surf. Coat. Technol.* **2010**, *204*, 2789–2796. [[CrossRef](#)]
17. Sun, Y. Tribocorrosion behavior of low temperature plasma carburized stainless steel. *Surf. Coat. Technol.* **2013**, *228*, S342–S348. [[CrossRef](#)]
18. Li, C.X.; Bell, T. Corrosion properties of plasma nitrided AISI 410 martensitic stainless steel in 3.5% NaCl and 1% HCl aqueous solutions. *Corros. Sci.* **2006**, *48*, 2036–2049. [[CrossRef](#)]
19. Corengia, P.; Ybarra, G.; Moina, C.; Cabo, A.; Broitman, E. Microstructure and corrosion behaviour of DC-pulsed plasma nitrided AISI 410 martensitic stainless steel. *Surf. Coat. Technol.* **2004**, *187*, 63–69. [[CrossRef](#)]
20. Rong, D.S.; Gong, J.M.; Jiang, Y.; Peng, Y. Effect of CO concentration on paraequilibrium gas carburization of 316L stainless steel. *Trans. Mater. Heat Treat.* **2015**, *36*, 204–209. (In Chinese)
21. Yang, Y.; Yan, M.; Zhang, Y.; Zhang, C.; Wang, X. Self-lubricating and anti-corrosion amorphous carbon/Fe₃C composite coating on M50NiL steel by low temperature plasma carburizing. *Surf. Coat. Technol.* **2016**, *304*, 142–149. [[CrossRef](#)]
22. Yang, Y.; Yan, M.; Zhang, Y.; Li, D.; Zhang, C.; Zhu, Y.; Wang, Y. Catalytic growth of diamond-like carbon on Fe₃C-containing carburized layer through a single-step plasma-assisted carburizing process. *Carbon* **2017**, *122*, 1–8. [[CrossRef](#)]
23. Yang, Y.; Yan, M.; Zhang, S.; Guo, J.; Jiang, D.; Li, D. Diffusion behavior of carbon and its hardening effect on plasma carburized M50NiL steel: Influences of treatment temperature and duration. *Surf. Coat. Technol.* **2018**, *333*, 96–103. [[CrossRef](#)]
24. Liu, R.; Wei, C.; Xu, A.; Yan, M.; Qiao, Y. Preparation and properties of “expanded” α phase layer on AISI 431 stainless steel. *Trans. Mater. Heat Treat.* **2017**, *38*, 165–172. (In Chinese)

25. Buhagiar, J.; Li, X.; Dong, H. Formation and microstructural characterisation of S-phase layers in Ni-free austenitic stainless steels by low-temperature plasma surface alloying. *Surf. Coat. Technol.* **2009**, *204*, 330–335. [[CrossRef](#)]
26. GB/T 24196-2009 *Corrosion of Metals and Alloys—Electrochemical Test Methods—Guidelines for Conducting Potentiostatic and Potentiodynamic Polarization Measurements*; Standardization Administration of the People's Republic of China: Beijing, China, 2009.
27. Orazem, M.E.; Tribollet, B. *Electrochemical Impedance Spectroscopy*; John Wiley & Sons: Hoboken, NJ, USA, 2008.



© 2019 by the authors. Licensee MDPI, Basel, Switzerland. This article is an open access article distributed under the terms and conditions of the Creative Commons Attribution (CC BY) license (<http://creativecommons.org/licenses/by/4.0/>).